Electronic states in Ge/Si quantum dots with type-II band alignment initiated by space-charge spectroscopy

A. I. Yakimov,* A. V. Dvurechenskii, A. I. Nikiforov, A. A. Bloshkin, A. V. Nenashev, and V. A. Volodin
Institute of Semiconductor Physics, Siberian Branch of the Russian Academy of Sciences, prospekt Lavrent'eva 13, 630090 Novosibirsk, Russia

(Received 23 September 2005; revised manuscript received 15 February 2006; published 27 March 2006)

Space-charge spectroscopy was employed to study electronic structure of a stack of four layers of Ge quantum dots (QD's) coherently embedded in an *n*-type Si(001) matrix. Evidence for an electron confinement in Si in the vicinity of neutral Ge dots was found. From the temperature- and frequency-dependent measurements the electron binding energy was determined to be ~50 meV. Existence of localized electronic states is explained by a modification of the conduction band alignment induced by inhomogeneous tensile strain in Si around the buried Ge dots. To support experimental results we performed numerical analysis of three-dimensional strain distribution and electronic structure of the sample under investigation. The strain distribution was found in terms of atomic positions using a valence-force-field model with a Keating interatomic potential. The electronic energy levels were calculated by solving a three-dimensional effective mass Schrödinger equation. The carrier confinement potential in this equation is modified by the strain distribution. The calculated confined eigenenergies agree with our experimental values deduced from the admittance spectroscopy. The data obtained in this work may serve as a guideline to interpret efficient photo- and electroluminescence as well as enhanced quantum efficiency of photodetectors and solar cells with Ge QD's stacked in a multilayer structure.

DOI: 10.1103/PhysRevB.73.115333 PACS number(s): 73.21.La, 73.20.At, 71.70.Fk, 81.07.Ta

I. INTRODUCTION

There are two main types of band-edge alignment, namely type I and type II, in heterostructures with semiconductor quantum dots (QD's). In type-I QD's, the band gap of the narrow-gap material lies entirely within the gap of the wide-gap semiconductor, and both electron and hole are confined inside the same region [Fig. 1(a)]. A typical example of type-I band-edge lineup is the InAs QD's in a GaAs matrix. For type-II QD's, the localization inside the dot occurs only for one of the charge carriers, i.e., electron (e) or hole (h), whereas the dot forms a potential barrier for the other particle [Fig. 1(b)]. A system like this is that of Ge/Si(001) dots formed by strain epitaxy, in which the holes are strongly confined in the Ge region, and the electrons are free in the Si conduction band. There are a large number of papers devoted to the experimental investigations of hole level scheme in the valence band of self-assembled Ge/Si QD's.[1–7] When an electron-hole pair is photoexcited, the hole is captured by the Ge dot and creates an attractive Coulomb potential, resulting in a binding of an electron in Si in the vicinity of the dot.[8,9] Thus, the common view is that the localization of electrons in type-II Ge/Si(001) QD's is possible only under interband optical excitation.

However, the above consideration disregards possible modification of the band structure due to inhomogeneous strain in the dots and the surrounding matrix, leading to an overestimation of the interband transition energies while analyzing numerous photoluminescence and absorption experiments. Recent calculations on $Ge_{1-x}Si_x/Si$ heterojunctions[10] and on Ge nanoclusters[11–13] coherently embedded in the Si host demonstrated that tensile strain in the surrounding Si causes splitting of the sixfold-degenerate Δ valleys (Δ_6) into the fourfold-degenerate in-plane Δ_4 valleys and the twofold-degenerate Δ_2 valleys along the [001] growth direction. Figure 1(d) represents a Fermi surface for the Si conduction band and illustrates the definition of Δ_4 and Δ_2 valleys. Since the average conduction band energy is unaffected by the uniaxial strain component, the Δ_4 and Δ_2 levels shift in the opposite directions with the Δ_2 band moving by twice the amount of the Δ_4 band. Thus the tensile strain in the Si in the vicinity of the Ge dot can reduce the band gap compared to that for bulk Si. The phenomena of a lowering of the Si band gap by 0.16 eV induced by inhomogeneous strain on top of the Ge island has been observed experimentally using locally resolved scanning tunneling microscopy by Meyer *et al.*[14] The lowest conduction band edge just above and below the Ge island is formed by the Δ_2 valleys yielding the triangle potential well for electrons in Si near the Si/Ge boundary [Fig. 1(c)]. Thus one can expect three-dimensional localization of electrons in the strained silicon near the Ge dots.[15]

Recently, Denker *et al.*[9] reported on the photoluminescence (PL) signal below the Ge band edge in Ge quantum dots overgrown with Si at low temperatures. The authors explained their results by electron confinement in the vicinity of the dots. Notice, in PL experiments, recombination of an electron with a hole occurs under condition such as the dot is charged with hole. Therefore one cannot discriminate between effect of strain-induced electron localization and a confinement in a Hartree potential of positively charged QD by using PL measurements only.

The localization energy of electron in a strain-induced potential well in a single Ge/Si QD was recently calculated to be as small as ~7 meV.[12] This value is expected to enlarge vastly in multilayer Ge/Si structures with vertical stacking of Ge islands due to accumulation of strain energy

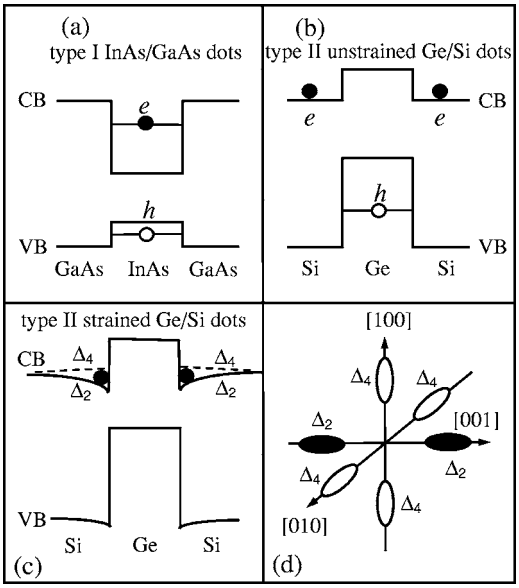

FIG. 1. Schematic overview of the band alignment in (a) type-I and (b) type-II QD's. (c) Band structure in Ge/Si(001) QD's modified by tensile strain. The conduction band (CB) in Si just above and below the Ge dot splits into Δ_4 and Δ_2 valleys. (d) Fermi surface in the Si conduction band.

from different dot layers in a stack and increase of the potential well depth. For a strongly localized electronic state, the wave vector **k** is no longer a good quantum number. As a result, the selection rules for the indirect transitions in stacked Ge/Si QD's would be substantially weakened. Probably this effect may explain efficient photo- and electroluminescence,[16–18] enhanced quantum efficiency of photodetectors,[19] and solar cells[20] with Ge QD's stacked in a multilayer structure. In this paper we present the experimental evidence for the electron confinement in the strained Si in the vicinity of Ge dots containing no holes.

II. SAMPLES AND EXPERIMENT

Samples were grown by molecular-beam epitaxy on an n^+-Si(001) substrate with a resistivity of 0.01 Ω cm doped with antimony up to a concentration of $\sim 10^{19}$ cm^{-3}. The growth temperature was 500 °C for all layers. A fourfold stack of Ge islands was inserted into the 0.8-μm epitaxial n-Si layer (Sb concentration $\sim 4\times 10^{16}$ cm^{-3}) at a distance of 0.5 μm from the substrate (Fig. 2). In order to reduce distortion of the electron confining potential by the potential of ionized impurities, a 10-nm thick undoped Si spacer was introduced between the topmost Ge layer and the n-type Si cover layer. To separate response from the dots, the reference sample was grown under conditions similar to the dot sample, except that no Ge was deposited.

The first and second Ge layers as well as the third and fourth Ge layers are separated by 3-nm Si spacers, while the distance between the second and third Ge layers is 5 nm. The Ge QD's formation was controlled by reflection high energy electron diffraction (RHEED) when the pattern changed from streaky to spotty. It is known that the Ge critical thickness decreases in the upper layers of a multilayer structure leading to the gradual increase of the island sizes within the island stacks from layer to layer.[21–24] This is due to the reduction of the strain caused by the lateral expansion of the lattice plane in the underlying island, giving rise to a reduction of the effective misfit.[21] To produce Ge islands having equal size in all layers it is necessary to adjust the Ge deposited amount in subsequent layers. As that has been realized previously by Le Thanh *et al.*[22,23] the Ge growth in each layer was stopped after the appearance of three-dimensional spots in the RHEED pattern. Ge nanoclusters fabricated by such a way demonstrate good vertical correlation and have almost equal size [Fig. 3(a)]. From cross-sectional transmission electron micrographs (TEM), we observe the Ge dots to be approximately 20–25 nm in lateral size and about 1.5 nm in height [Fig. 3(a)]. The scanning tunneling microscopy

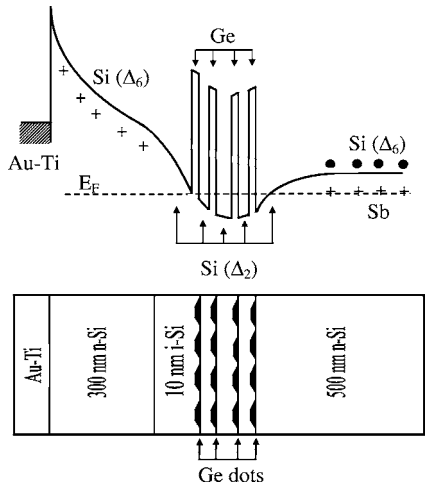

FIG. 2. A schematic conduction band diagram of the Si Schottky diode containing a stack of Ge QD's and a sketch of the sample structure. The n^+-Si substrate is not shown.

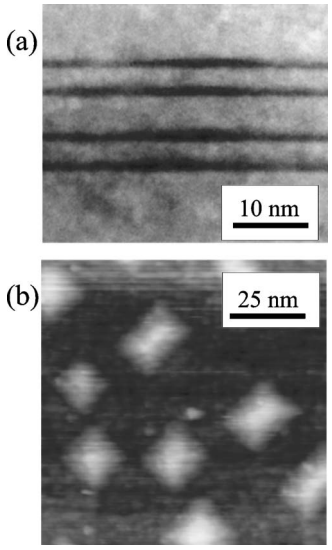

FIG. 3. (a) Cross-sectional TEM image of a stack of four layers of Ge islands deposited on Si(001) at 500 °C. (b) Plan-view STM image of topmost uncapped Ge layer.

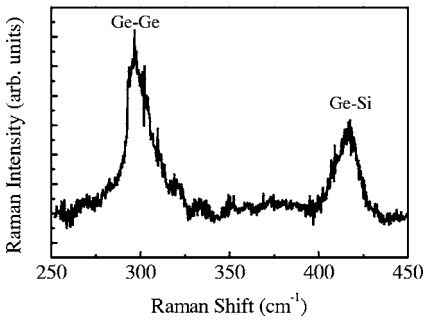

FIG. 4. Raman spectrum of Ge QD sample.

(STM) of a sample without the Si cap layer showed that the Ge islands have a shape of "hut" clusters [Fig. 3(b)]. The density of the dots is $n_{QD} \simeq 1 \times 10^{11}$ cm^{-2}.

The Raman spectra were measured at room temperature using a computer-controlled setup based on a DFS-52 spectrometer (LOMO, St. Petersburg); an Ar^+ laser ($\lambda = 514.5$ nm) was used as the pump for the Raman process. We used quasi-backscattering geometry, the incident radiation was polarized along $\langle 100 \rangle$ crystallographic direction, and the scattered light was detected in $\langle 010 \rangle$ polarization. The chosen configuration is allowed for the scattering by longitudinal optical phonons in Ge and Si and forbidden for the two-phonon scattering by transverse acoustical phonons in the Si substrate. This enabled us to avoid confusions encountered when interpreting Raman spectra in Ge/Si heterostructures.[25]

For the capacitance and conductance measurements, Ti-Au Schottky gates were deposited at room temperature on top of the samples through a shadow mask. The area of the Au-Ti contacts was $S \simeq 7.5 \times 10^{-3}$ cm^2. The back contact was formed by alloying indium to the n^+-type Si substrate. Figure 2 schematically displays the conduction band of the QD sample at zero bias. The admittance was measured using a Fluke PM6306 RCL meter in the frequency range $f = 10-1000$ kHz at temperatures from 10 to 100 K. The amplitude of the ac modulation voltage was 50 mV.

III. RESULTS AND DISCUSSION

A. Raman spectroscopy

The samples were first characterized by Raman spectroscopy to estimate Ge-Si intermixing effect in Ge QD's (Fig. 4). A peak observed at ~ 300 cm^{-1} originates from the optical vibration of Ge-Ge bonds in Ge islands. Another feature at ~ 420 cm^{-1} corresponds to the local Ge-Si vibrations. Based on Raman measurements the Ge-Si intermixing effect can be found from the ratio of the integrated intensities of the Ge-Ge and Ge-Si peaks,[26]

$$\frac{I_{\text{Ge-Ge}}}{I_{\text{Si-Ge}}} = \alpha \frac{x}{2(1-x)}, \tag{1}$$

where x is the Ge content in the nanoclusters and α is a constant which depends on the experimental conditions. We initially checked the validity of Eq. (1) for a number of thin SiGe layers with a known Ge content.[7] In this way, we determined a coefficient α of 2.2 for our experimental conditions. Analysis shows that the average Ge content in the dots is ~ 0.7.

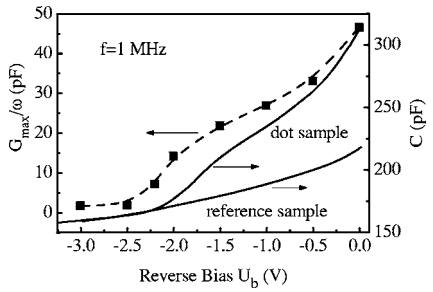

FIG. 5. Capacitance-voltage characteristics measured at modulation frequency of 1 MHz and at $T = 77$ K for the reference and dot samples. This figure shows also the dependence of the amplitude $G_{\max}/\omega$ of the peak B (see Fig. 7) on the bias voltage (left scale).

B. Capacitance-voltage characteristics

Figure 5 shows experimental capacitance-voltage (C-V) characteristics for the reference and the dot samples. The traces were recorded at $T = 77$ K and at the modulation frequency of 1 MHz. At such frequency and temperature, the C-V characteristics are frequency independent, which is a manifestation of an equilibrium of the charging/discharging process. The dependence of the capacitance on voltage for the reference sample shows no specific features and has the form of the conventional C-V characteristic of an n-type Schottky diode. For the dot sample, we observe a steplike structure caused by an additional capacitance, which we associate with the negative charge accumulation in the dot layers between the stacked Ge islands. Due to the n-type doping in the Si matrix, the stacks of Ge QD's will be charged by electrons at a zero bias. When a reverse bias is applied to the diode, the electrons are gradually swept out. At $U_b \gtrsim 2$ V electrons escape from the dots and the latter become neutral.

Due to the thicker central Si spacer as compared with the frontier Si layers in stacks, it is reasonable to expect that the ground state of electrons would be localized in the middle of the structure while the first and the third Si layers are needed to accumulate the strain and to increase the potential well for electrons in the center.[27] As a first approximation, the width of the capacitance plateau ΔU_b can be used to estimate the average number of electrons accumulated in each stack by $N_e = (C/qSn_{QD})\Delta U_b$, where $q > 0$ is the elementary charge, C is the capacitance of the plateau, S is the contact area, and n_{QD} is the dot density in a single QD layer. For $\Delta U_b \sim 2$ V, $C \sim 250$ pF, $n_{QD} = 10^{11}$ cm^{-2}, we estimate $N_e \approx 4$. The degeneracy factor for the electron ground state is equal to 4; 2 comes from two different spin orientations and 2 from two equivalent Δ_2 valleys. For a uniform array of QD's, this means that, at $U_b = 0$ V, the ground state of each stack is completely filled with electrons; the highest energy states of the dots are empty and cannot be measured by space-charge spectroscopy. However, in a QD system with small interlevel spacing and large energy dispersion caused by the variation

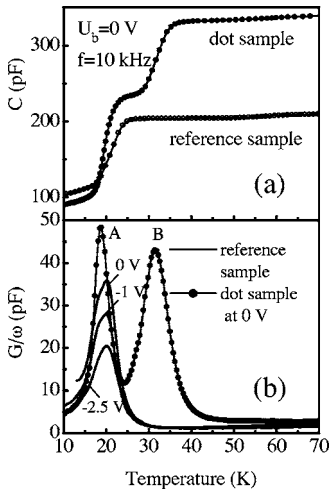

FIG. 6. Temperature dependencies of (a) capacitance and (b) conductance measured at bias voltage $U_b=0$ V and modulation frequency of 10 kHz for the reference and dot samples.

of the dot sizes, electrons can populate excited states and contribute to the ac response.

C. Admittance spectroscopy

The QD contribution to the capacitance disappears at temperatures below 30–40 K [Fig. 6(a)] due to "freezing" the electrons in the Δ_2 bound states in the strain Si. The corresponding step on the temperature dependence of capacitance is accompanied by the conductance maximum [peak *B* in Fig. 6(b)] which is not seen for the reference sample. Thus we may attribute the conductance peak *B* to the ac response of electrons confined in stacks of Ge/Si QD's. This assumption gets further support from bias-dependent measurements. Figure 7 shows evolution of the conductance maxima with applied reverse bias. With increasing reverse bias, the position of peak *B* shifts towards higher temperatures, its amplitude gradually decreases and the peak disappears at voltages $|U_b|>2.2$ V just after the ending of the capacitance plateau in *C-V* characteristic (Fig. 5). For the Schottky diodes with QD's, the $G(T)$ traces should exhibit maximum whose amplitude $G_{\max}/\omega$ is proportional to the number of electrons being exchanged between localized and extended states.[28,29]

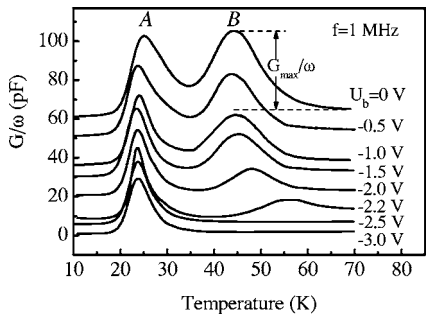

FIG. 7. Conductance spectra of the QD sample at the frequency of 1 MHz under different bias voltages. Each curve has been offset for clarity.

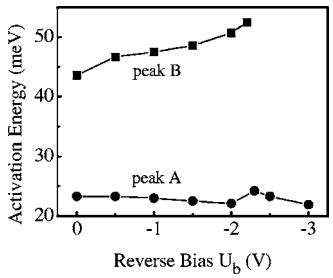

FIG. 8. Bias dependent activation energies.

In Fig. 5 we plot the amplitude of the peak *B* as a function of voltage. It is important that $G_{\max}/\omega$ strictly follows the capacitance-voltage characteristic, giving evidence that both capacitance and conductance are related to the same phenomena of QD charging/discharging process.

Peak *A* is observed in both samples. In contrast to that of the peak *B*, the position of peak *A* is not changed with applied bias (Fig. 7) indicating a nearly constant activation energy for the corresponding ac response. Similar to Ref. 30, we assign peak *A* to a dopant-related admittance signal associated with the carrier freeze-out effect.[31] As temperature decreases, the major free carrier concentration goes down and the epitaxial layer becomes an insulator, resulting in changing the resonance condition for the equivalent circuit seen by the RCL meter. At low temperatures ($T<20$ K), the sample capacitance is not determined by the width of the space-charge region but the total thickness of the epitaxial layer. In this case the resonant condition for the conductance maximum can be expressed as[31] $f=AT_{\max}^3 \exp(-E_d/2kT)$, where f is the modulation frequency, A is a temperature-independent prefactor, E_d is the donor ionization energy for no compensation, and $T_{\max}$ is the temperature which corresponds to the maximum value of conductance. An Arrhenius plot of $f/T_{\max}^3$ vs $1/T_{\max}$ would give the energy $E_d/2$. From the frequency-dependent measurements we found the activation energy for the peak *A* to be about 20 meV (Fig. 8) which is nearly half of the ionization energy of Sb in Si ($E_d^{\mathrm{Sb}}\approx 40$ meV).

Typical conductance spectra measured at different frequencies are shown in Fig. 9. Admittance signal originated from electron traps can be used to extract the trap energy level. For a given measurement frequency $\omega=2\pi f$, the conductance reaches a maximum at a temperature $T_{\max}$ which corresponds to the condition $e_n(T_{\max})\approx\omega/2$, where $e_n=e_0\exp(-E_a/kT)$ is the emission rate of electrons from the

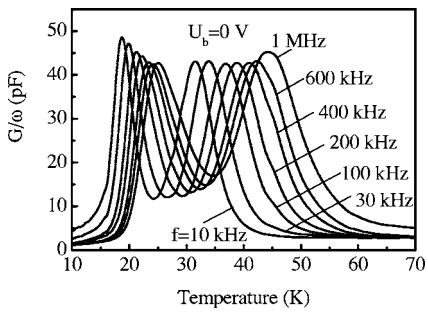

FIG. 9. Conductance spectra of the QD sample at the bias voltage of 0 V under different modulation frequencies.

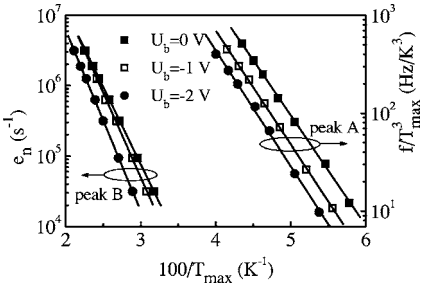

FIG. 10. The Arrhenius plots of the electron emission rate e_n and of the combination $f/T^3_{\max}$ (see text) obtained from *G-T* spectra with different bias voltages.

bound to extended states which depends on the electron binding energy E_a.[29] Just as in Ref. 32, we assume the pre-exponential factor e_0 to be temperature independent, because it is not *a priori* clear how the e_0 depends on temperature for shallow levels in QD's. Thus, by measuring $G(T)$ dependencies at various ω, the activation energies of the electron emission rate can be deduced from the Arrhenius plots of $e_n(T_{\max})$ vs $1/T_{\max}$. Arrhenius plots necessary for deriving the activation energy are depicted in Fig. 10. The activation energies of the electron emission rate were found from the slope of the approximating straight lines. The linear correlation coefficients of all the lines are larger than 0.9999. The resulting values of E_a are shown in Fig. 8 as a function of reverse bias voltage. We suggest that the activation energy of about 50 meV found for the peak *B* represents the average energy level of electrons in stacks of Ge/Si QD's relative to the conduction band edge of unstrained Si.

The activation energy for the peak *B* increases with increasing of the bias voltage, while that remains nearly constant for the dopant-related peak *A*. With increasing of the reverse bias, the chemical potential scans through the density of electron states in the QD layers. At higher reverse bias, the chemical potential crosses deeper states in the dots. In QD's, in which conclusively higher energy levels than the ground state are occupied, the dependence of the activation energy on the QD occupation is usually related to the state-filling effect.[3,33] For the sample under investigation the interlevel spacing is small enough ($\sim$10 meV, see Sec. III D) and compared with the variation of the activation energy with bias voltage. Thus, the change of the activation energy for the peak *B* with bias may be attributed both to the spread of the electron eigenenergy due to size distribution of QD's and the state-filling effect.

D. Theoretical consideration

To support experimental results we performed numerical analysis of three-dimensional (3D) strain distribution and electronic structure of the sample under investigation. The stacked QD structure is modeled by fourfold stacked GeSi QD's aligned along the growth direction z and separated by Si. Each GeSi QD has a truncated-pyramid shape with base orientation along [100] (x) and [010] (y) directions. The length of the base side was 23 nm, the height is 1.5 nm. Each pyramid lies on a 4.5 monolayer (ML) GeSi wetting layer and contains 30% Si atoms randomly distributed within QD. The size of computational cell (GeSi island plus Si environment) is $50a \times 50a \times 50a$ along x, y, and z axes, respectively, where a=5.431 Å is the Si lattice constant. The size of the pyramid base is $28a \times 28a$, the height is $2a$. Calculated strain distribution was then scaled by a factor of 1.5 in all three dimensions to reach realistic sizes of Ge/Si island (base length of $\approx$23 nm and height of $\approx$1.5 nm).

The strain distribution was found in terms of atomic positions, using a valence-force-field (VFF) model with a Keating interatomic potential,[34,35] previously adopted for self-assembled QD's with different shapes.[13,36–40] In comparison with the finite-difference[41] and finite-element methods,[11,42–44] which are also often used for the strain calculations of QD's, the advantage of the VFF model is that the strain energies and the positions of all the atoms in a supercell can be obtained. The elastic energy W is given by

$$W = \frac{3}{16}\sum_i \sum_j \frac{\alpha_{ij}}{d_{ij}^2}[(\mathbf{r}_i - \mathbf{r}_j)^2 - d_{ij}^2]^2 + \frac{3}{8}\sum_i \sum_{j>k} \frac{\beta_{ijk}}{d_{ij}d_{ik}} \times \left[(\mathbf{r}_i - \mathbf{r}_j)(\mathbf{r}_i - \mathbf{r}_k) + \frac{d_{ij}d_{ik}}{3}\right]^2, \quad (2)$$

where the indices i, j, and k enumerate the atoms, the index i run over all atoms, j in the first sum runs over the nearest neighbors of the ith atom, and the pair of indices (j,k) in the second sum runs over all pairs of nearest neighbors of the ith atom; $\mathbf{r}$ is the atomic position, d_{ij} is the unstrained bond length, and α_{ij} and β_{ijk} are the force constants in the Keating model. The parameters of the VFF model (atomic force constants for bond stretching, bond bending and unstrained bond lengths) we used are the same as in Refs. 13 and 39. The problem of finding a set of atomic positions that minimizes W was solved using a Green's function approach to the "atomistic" elastic problem developed by Nenashev and Dvurechenskii and applied previously to a single pyramidal Ge island in Si.[39,45] The main advantage of this approach is that the final results are insensitive to the position of the boundary of the atomic cluster chosen. To obtain strain distribution in a stacked island arrangement, the calculated strain fields of single islands are superimposed and added in real space. This approach overestimates the strain in Si by only 10%.[11] In order to check whether the calculation volume is large enough to give the proper (size-independent) result we performed numerical analysis also for smaller computational cells ($32a \times 32a \times 50a$ and $32a \times 32a \times 32a$) and found that the strain distribution does not depends on the size of supercell to within 5% of accuracy.

It is natural to expect that the maximum strain is realized in the middle of the stack.[11] The calculated strain components along the z and x directions through the center of symmetry of a fourfold stack of $Ge_{0.7}Si_{0.3}$ islands is shown in Fig. 11. The positive strain values correspond to tensile strain and the negative ones to compressive strain. The tension in the Si above and below GeSi islands is evident. In the lateral direction the strain in Si relaxes from the center at a scale comparable to the diameter of underlying GeSi island and then changes its sign, demonstrating that the Si is laterally compressed near the edges of GeSi islands. Above the stack,

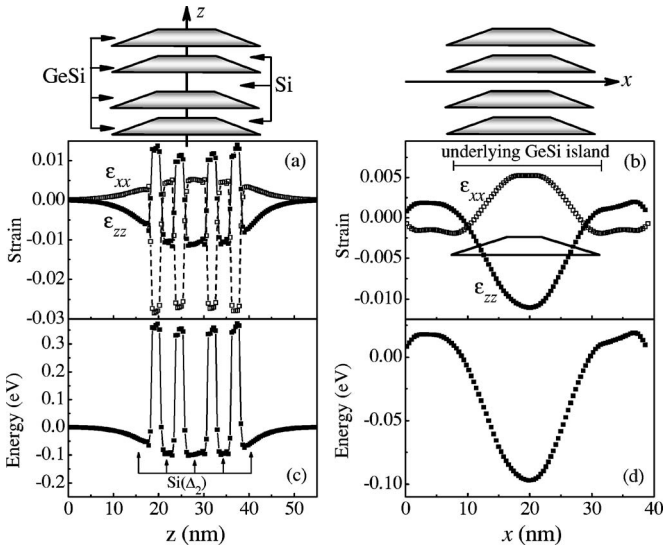

FIG. 11. Strain tensor components ϵ_{zz} and ϵ_{xx} ($\epsilon_{yy}=\epsilon_{xx}$) for a fourfold $Ge_{0.7}Si_{0.3}$ island stack (shown on top panels) along (a) the z axis and (b) the x axis. In a latter case the strain profiles are plotted for the central Si separation layer above the tip of GeSi island. (c) and (d) The strain-modified confinement potential for electrons with respect to the conduction band edge of unstrained Si along the same directions.

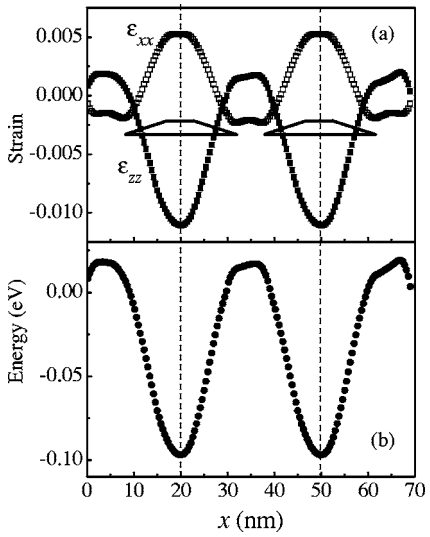

FIG. 12. (a) zz and xx components of the strain tensor for two $Ge_{0.7}Si_{0.3}$ island stacks separated by 30 nm in the layer plane. (b) The strain-modified confinement potential for electrons. All profiles are plotted along the x axis as in Figs. 11(b) and 11(d).

strain goes to zero with z over a length of about $\ell=15$ nm.

Now let us consider the strain-modified conduction band-edge diagram at the Δ_2 valleys in which the electron localization is expected. The 3D potential energy distribution of electrons in Δ_2 states with respect to the unstrained Si conduction band-edge can be expressed as[46]

$$V(\mathbf{r}) = \Delta E_c x(\mathbf{r}) + \Xi_d \mathrm{Tr}[\epsilon(\mathbf{r})] + \Xi_u \epsilon_{zz}(\mathbf{r}), \tag{3}$$

where ΔE_c is conduction band offset between unstrained Si and GeSi, $x(\mathbf{r})=1$ on conditions that the vector $\mathbf{r}$ points to the atom inside GeSi island, otherwise $x(\mathbf{r})=0$; Ξ_d and Ξ_u are the deformation potentials. The quantity $\left(\Xi_d+\frac{1}{3}\Xi_u\right)$ corresponds to a_c, the hydrostatic deformation potential for the conduction band. $\mathrm{Tr}[\epsilon(\mathbf{r})]$ is equal to $\epsilon_{xx}+\epsilon_{yy}+\epsilon_{zz}$ which is hydrostatic component of the strain. Values of deformation potentials a_c and Ξ_u are taken from Ref. 46. The conduction band offset between unstrained Si and Ge_xSi_{1-x} can be found by subtracting the Si bandgap (E_g^{Si}) from the sum of the valence band offset (ΔE_v) and the bandgap of unstrained Ge_xSi_{1-x} (E_g^{GeSi}),

$$\Delta E_c = E_g^{\mathrm{GeSi}} + \Delta E_v - E_g^{\mathrm{Si}}. \tag{4}$$

The linear interpolation of the valence band offset in a Ge/Si heterostructure with respect to Ge composition x was justified in Refs. 47 and 48. For pure Ge on Si(001), theoretical and experimental studies yields the valence band offset to be around $\sim$0.7 eV.[48–51] Thus we can write

$$\Delta E_v = 0.7x[\mathrm{eV}]. \tag{5}$$

The linear interpolation is less adequate for the conduction band offset, which varies nonlinearly with Ge content.[46] The band gap for an unstrained Ge_xSi_{1-x} alloy was measured by Weber and Alonso using photoluminescence spectroscopy at 4.2 K.[52] According to Weber and Alonso,

$$E_g^{\mathrm{GeSi}} = 1.155 - 0.43x + 0.206x^2[\mathrm{eV}] \tag{6}$$

at the Δ point. Using Eqs. (4)–(6), we obtain $\Delta E_c=0.29$ eV for $E_g^{\mathrm{Si}}=1.15$ eV (at $T=4.2$ K) and $x=0.7$. The final conduction band-edge alignment along the z and x directions through the center of symmetry of a fourfold stack of $Ge_{0.7}Si_{0.3}$ islands is shown in Fig. 11. One can see that potential well for electrons is more shallow in the layer plane ($\sim$100 meV) and just its depth determines the electron binding energy.

An important problem is the overlapping of strain fields in the lateral direction. The average distance between the dots in the layer plane is $d=30-40$ nm. The strains from different QD's may add up, thereby forming a two-dimensional (2D) potential well for electrons. In Fig. 12 we plot the calculated strain components and the electron potential profile at Δ_2 point along the x axis for two island stacks separated by $d=30$ nm. Clearly there are two well-defined potential wells for electrons separated by a potential barrier.

The electron bound states are found by numerical solving the 3D Schrödinger equation using the effective-mass approximation,

$$\left(\frac{\hat{p}_x^2+\hat{p}_y^2}{2m_{xy}} + \frac{\hat{p}_z^2}{2m_z}\right)\psi + V\psi = E\psi, \tag{7}$$

where $V=V(\mathbf{r})$ is defined by Eq. (3). We took the values of longitudinal and transversal effective masses at the Δ minimum in Si as m_z and m_{xy}, correspondingly; so $m_z=0.92m_0$ and $m_{xy}=0.19m_0$ (m_0 is the free electron mass). The size of the computational cell is $62\times62\times120$ along x, y, and z axes, respectively, in unit of three-fourths the lattice constant of bulk Si, i.e., $25.2\times25.2\times48.9$ nm^3. To calculate the energy levels and electron wave functions we employ the free-

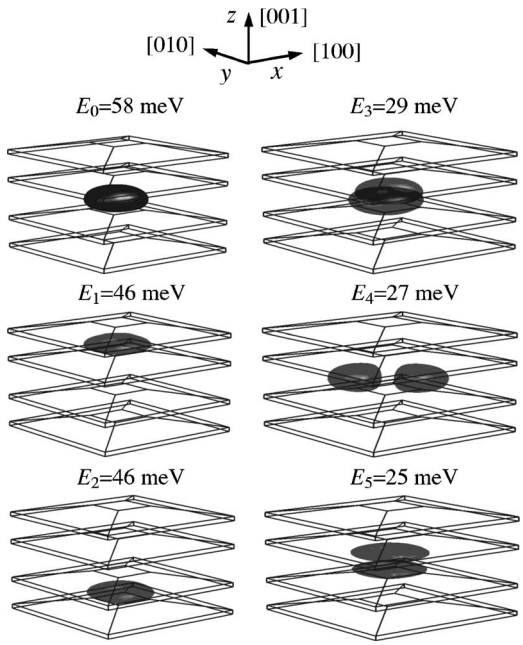

FIG. 13. Three-dimensional view of the isosurface of the electron charge density for the six lowest conduction states. The isosurface level is selected as $1/e$ ($e=2.71\,828\ldots$) of the maximum wave-function amplitude $|\psi_{max}(\mathbf{r})|$. The probability of finding the electron inside is 70–77 % dependent on the state. E_i is the single-electron binding energy of the ith state, determined with the error of ±1 meV. The pyramid base size is 23×23 nm^2.

relaxation method.[53,54] Let us consider the time-dependent Schrödinger equation $i\hbar\partial\psi/\partial t=H\psi$. Introducing the imaginary-time parameter $\tau=it$ we obtain the τ -dependent form

$$-\partial\psi/\partial\tau=H\psi. \tag{8}$$

Equation (8) is solved numerically for positive τ using a finite-difference method with initial condition $\psi|_{\tau=0}=\psi_0$ (ψ_0 is an arbitrary seed wave function). One can expand the ψ over the eigenstates ϕ_i of the time-independent Schrödinger equation $H\phi=E\phi$ and express the evolution of ψ with τ in the form $\psi(\tau)=\Sigma_i c_i\phi_i\exp(-E_i\tau/\hbar)$. When $\tau\to\infty$ the terms with large E_i disappear, and $\psi(\tau)\to c_0\phi_0\exp(-E_0\tau/\hbar)$. With a proper truncation of the ground state ϕ_0 in the initial function ψ one can find the first excited state and so on.

In Fig. 13 we show the isosurface plots of the charge density $|\psi_i(\mathbf{r})|^2$ for the first six electronic states. The isosurface level is selected as $1/e$ ($e=2.71\,828\ldots$) of the maximum wave-function amplitude $|\psi_{max}(\mathbf{r})|$. The lowest three electron states are an s-like state located in different Si spacers, while the next three are p-like states localized along [001], [110], and [$\bar{1}$10], respectively. As expected, the electron ground state is really confined in the middle of the stack. The electron binding energy for the lowest state is found to be about 58 meV, which is quite close to the experimental data. The next two states have the energy of ~46 meV and located by 12 meV above the ground state level. The electron wave functions are strongly localized near the tip of GeSi islands. The in-plane size of $|\psi_i(\mathbf{r})|^2$ is ~10 nm, i.e., smaller than the average interdot distance d in the layer plane xy. This implies that the wave functions of the neighboring dots do not overlap and we have a 3D confinement of isolated electron states instead of a 2D electron gas. To check this assumption in more detail we calculate the wave function overlapping $J_{ij}=\int\psi_i(\mathbf{r})\psi_j^*(\mathbf{r})d\mathbf{r}$, where ψ_i and ψ_j are the ground state electron wave functions of the quantum dots distributed laterally in the growth plane. For $d=30$ nm, we obtain actually negligible value $J_{ij}=2\times 10^{-6}$.

IV. SUMMARY

Using the admittance spectroscopy, we have demonstrated the effect of electron localization in vertically stacked $Ge_{0.7}Si_{0.3}$ self-assembled quantum dots coherently embedded in an n-type Si matrix. The electron binding energy was found to be about 50 meV. This effect is related to the appearance of the three-dimensional potential well in the Si conduction band in the vicinity of GeSi nanoclusters caused by strain-induced splitting of the sixfold-degenerate Δ valleys. The electron energy levels were calculated by solving the three-dimensional effective mass Schrödinger equation using the free-relaxation method. The carrier confinement potential in this equation is modified by strain distribution. The calculated electron energies agree well with the experimental data.

ACKNOWLEDGMENTS

The authors are much obliged to A. K. Gutakovskii for TEM measurements and S. A. Teys for STM experiments. We acknowledge the support of RFBR (Grant No. 06-02-16143), State Contract 02.442.11.7282, and Integration Project of SB RAS (Grant No. 101). A.V.N. is also grateful to Foundation "Dinastiya."

*Electronic address: yakimov@isp.nsc.ru

[1] S. K. Zhang, H. J. Zhu, F. Lu, Z. M. Jiang, and X. Wang, Phys. Rev. Lett. **80**, 3340 (1998).

[2] K. Schmalz, I. N. Yassievich, P. Schittenhelm, and G. Abstreiter, Phys. Rev. B **60**, 1792 (1999).

[3] C. M. A. Kapteyn, M. Lion, R. Heitz, D. Bimberg, C. Miesner, T. Asperger, K. Brunner, and G. Absreiter, Appl. Phys. Lett. **77**, 4169 (2000).

[4] C. Miesner, T. Asperger, K. Brunner, and G. Abstreiter, Appl. Phys. Lett. **77**, 2704 (2000).

[5] H. Zhou, S. Huang, Y. Rao, Z. Jiang, and F. Lu, Solid State Commun. **125**, 161 (2003).

[6] A. I. Yakimov, A. V. Dvurechenskii, A. I. Nikiforov, and G. Yu. Mikhalev, JETP Lett. **80**, 321 (2004).

[7] A. I. Yakimov, A. V. Dvurechenskii, V. A. Volodin, M. D. Efremov, A. I. Nikiforov, G. Yu. Mikhalyov, E. I. Gatskevich, and G. D. Ivlev, Phys. Rev. B **72**, 115318 (2005).
[8] A. I. Yakimov, A. V. Dvurechenskii, A. I. Nikiforov, O. P. Pchelyakov, and A. V. Nenashev, Phys. Rev. B **62**, R16283 (2000).
[9] U. Denker, M. Stoffel, O. G. Schmidt, and H. Sigg, Appl. Phys. Lett. **82**, 454 (2003).
[10] V. Ya. Aleshkin and N. A. Bekin, J. Phys.: Condens. Matter **9**, 4841 (1997).
[11] O. G. Schmidt, K. Eberl, and Y. Rau, Phys. Rev. B **62**, 16715 (2000).
[12] A. I. Yakimov, N. P. Stepina, A. V. Dvurechenskii, A. I. Nikiforov, and A. V. Nenashev, Semicond. Sci. Technol. **15**, 1125 (2000).
[13] J. H. Seok and J. Y. Kim, Appl. Phys. Lett. **78**, 3124 (2001); J. Y. Kim and J. H. Seok, Mater. Sci. Eng., B **89**, 176 (2002).
[14] T. Meyer, M. Klemenc, and H. von Kanel, Phys. Rev. B **60**, R8493 (1999).
[15] Notice that similar arguments were also applied to design Si/SiGe-based modulation-doped quantum well structures with the motivation to improve electron and hole mobility. For a review, see, F. Schäffler, Semicond. Sci. Technol. **12**, 1515 (1997).
[16] N. D. Zakharov, V. G. Talalaev, P. Werner, A. A. Tonkikh, and G. E. Cirlin, Appl. Phys. Lett. **83**, 3084 (2003).
[17] K. W. Sun, S. H. Sue, and C. W. Liu, Physica E (Amsterdam) **28**, 525 (2005).
[18] W.-H. Chang, A. T. Chou, W. Y. Chen, H. S. Chang, T. M. Hsu, Z. Pei, P. S. Chen, S. W. Lee, L. S. Lai, S. C. Lu, and M.-J. Tsai, Appl. Phys. Lett. **83**, 2958 (2003).
[19] M. El Kurdi, P. Boucaud, S. Sauvage, G. Fishman, O. Kermarrec, Y. Campidelli, D. Bensahel, G. Saint-Girons, G. Patriarche, and I. Sagnes, Physica E (Amsterdam) **16**, 523 (2003).
[20] A. Alguno, N. Usami, T. Ujihara, K. Fujiwara, G. Sazaki, K. Nakajima, and Y. Shiraki, Appl. Phys. Lett. **83**, 1258 (2003).
[21] J. Tersoff, C. Teichert, and M. G. Lagally, Phys. Rev. Lett. **76**, 1675 (1996).
[22] V. Le Thanh, V. Yam, P. Boucaud, F. Fortuna, C. Ulysse, D. Bouchier, L. Vervoort, and J.-M. Lourtioz, Phys. Rev. B **60**, 5851 (1999).
[23] V. Le Thanh, V. Yam, P. Boucaud, Y. Zheng, and D. Bouchier, Thin Solid Films **369**, 43 (2000).
[24] K. Brunner, Rep. Prog. Phys. **65**, 27 (2002).
[25] A. V. Kolobov, J. Appl. Phys. **87**, 2926 (2000).
[26] P. M. Mooney, F. H. Dacol, J. C. Tsang, and J. O. Chu, Appl. Phys. Lett. **62**, 2069 (1993); J. C. Tsang, P. M. Mooney, F. Dacol, and J. O. Chu, J. Appl. Phys. **75**, 8098 (1994).
[27] This statement will be reproduced theoretically in Sec. III D.
[28] P. N. Brunkov, A. R. Kovsh, V. M. Ustinov, Yu. G. Musikhin, N. N. Ledentsov, S. G. Konnikov, A. Polimeni, A. Patané, P. C. Main, L. Eaves, and C. M. A. Kapteyn, J. Electron. Mater. **28**, 486 (1999).
[29] W.-H. Chang, W. Y. Chen, M. C. Cheng, C. Y. Lai, T. M. Hsu, N.-T. Yeh, and J.-I. Chyi, Phys. Rev. B **64**, 125315 (2001).
[30] V. I. Zubkov, C. M. A. Kapteyn, A. V. Solomonov, and D. Bimberg, J. Phys.: Condens. Matter **17**, 2435 (2005).
[31] D. V. Singh, R. Kim, T. O. Mitchell, J. L. Hoyt, and J. F. Gibbons, J. Appl. Phys. **85**, 985 (1999).
[32] W.-H. Chang, W. Y. Chen, T. M. Hsu, N.-T. Yeh, and J.-I. Chyi, Phys. Rev. B **66**, 195337 (2002).
[33] M. Geller, C. Kapteyn, L. Müller-Kirsch, R. Heitz, and D. Bimberg, Appl. Phys. Lett. **82**, 2706 (2003).
[34] P. N. Keating, Phys. Rev. **145**, 637 (1966).
[35] R. Martin, Phys. Rev. B **1**, 4005 (1970).
[36] M. A. Cusack, P. R. Briddon, and M. Jaros, Phys. Rev. B **54**, R2300 (1996).
[37] C. Pryor, J. Kim, L. W. Wang, A. J. Williamson, and A. Zunger, J. Appl. Phys. **83**, 2548 (1998).
[38] L. W. Wang, J. Kim, and A. Zunger, Phys. Rev. B **59**, 5678 (1999).
[39] A. V. Nenashev and A. V. Dvurechenskii, JETP **91**, 497 (2000).
[40] Y. Kikuchi, H. Sugii, and K. Shintani, J. Appl. Phys. **89**, 1191 (2001).
[41] M. Grundmann, O. Stier, and D. Bimberg, Phys. Rev. B **52**, 11969 (1995).
[42] T. Benabbas, P. Francois, Y. Androussi, and A. Lefebvre, J. Appl. Phys. **80**, 2763 (1996).
[43] T. Benabbas, Y. Androussi, and A. Lefebvre, J. Appl. Phys. **86**, 1945 (1999).
[44] T. Saito, T. Nakaoka, T. Katitsuka, Y. Yoshikuni, and Y. Arakawa, Physica E (Amsterdam) **26**, 217 (2005).
[45] A. V. Dvurechenskii, A. V. Nenashev, and A. I. Yakimov, Nanotechnology **13**, 75 (2002).
[46] C. G Van de Walle, Phys. Rev. B **39**, 1871 (1989).
[47] C. G Van de Walle and R. M. Martin, Phys. Rev. B **34**, 5621 (1986).
[48] L. Colombo, R. Resta, and S. Baroni, Phys. Rev. B **44**, 5572 (1991).
[49] C. G Van de Walle and R. M. Martin, J. Vac. Sci. Technol. B **4**, 1055 (1986).
[50] G. P. Schwartz, M. S. Hybertsen, J. Bevk, R. G. Nuzzo, J. P. Mannaerts, and G. J. Gualtieri, Phys. Rev. B **39**, 1235 (1989).
[51] J. F. Morar, P. E. Batson, and J. Tersoff, Phys. Rev. B **47**, 4107 (1993).
[52] J. Weber and M. I. Alonso, Phys. Rev. B **40**, 5683 (5683).
[53] A. A. Kiselev and U. Rössler, Phys. Rev. B **50**, 14283 (1994).
[54] F. B. Pedersen and Yia-Chung Chang, Phys. Rev. B **53**, 1507 (1996).